THE PUBLISHING HOUSE
OF THE ROMANIAN ACADEMY

PROCEEDINGS OF THE ROMANIAN ACADEMY, Series A,
Volume 11, Number 1/2010, pp. 33–40

DIRECT AND INVERSE PROBLEMS FOR THE EVERSION OF A SPHERICAL SHELL

Raluca I. ROŞCA, Corina S. DRAPACA

Department of Engineering Science and Mechanics, Pennsylvania State University
Corresponding author: Corina S. DRAPACA, 212 Earth-Engineering Sciences Building, University Park, PA 16802, USA,
Fax:+1.814.863.7967, E-mail: csd12@psu.edu

Motivated by an interest in material parameter determination for a structure with residual stresses, we revisit the classical eversion problem of a spherical shell, as studied by Ericksen, 1955 and more recently Johnson and Hoger, 1993. The spherical shell is made of an isotropic, incompressible, hyperelastic, Mooney-Rivlin material. In the direct problem, we examine the dependence of the elasticity tensor coefficients on residual and initial stresses and represent it for three numerical cases. In the inverse problem, we analyse the effect of measurement uncertainties on the determined values of material parameters and we suggest an experimental protocol that allows for a robust recovery of these parameters.

Key words: Inverse problems; Eversion; Mooney-Rivlin; Residual stresses.

1. INTRODUCTION

Diagnostic radiology is an exciting and rapidly expanding multi-disciplinary field of clinical medicine which links medicine to science and engineering. It enables noninvasive imaging and investigation of structure and function of the human body, and a unique insight into disease processes in vivo. In particular, computed tomography (CT), magnetic resonance (MR), or other biomedical imaging modalities can be used for inspecting the inner surfaces of hollow structures such as the colon and stomach. However, traditional visualization techniques can present only a very small portion of inner surfaces in one view, due to the limitations of the operator's perspective and of the field of view with virtual endoscopy. Thus, navigation is typically required in a visualization session, which is time-consuming, tedious, and error-prone particularly when features of interest are hidden [3, 5].

Among the many methods proposed in the literature to overcome the above mentioned difficulties in visualizing anatomical cavities, the digital eversion of a hollow structure introduced very recently by Zhao *et al.* [8] is the most promising. As the name of this technique suggests, the turning inside out of a structure is done via a computer. The primary advantages of digital eversion over conventional virtual endoscopy include the direct visualization of a larger portion of the inner surface and the close correlation to the important anatomical features, without the need for difficult and time-consuming navigation. In addition, the digital eversion method combined with an appropriate mechanical model of an anatomical structure could help in finding the mechanical parameters of the imaged structure which contain important information about its pathology since tumors are harder than the surrounding normal tissue. Thus, digital eversion with the help of mechanics can help improve screening, diagnosis, surgical planning and medical education.

Given the relevance that the eversion problem of a spherical shell might have to modern medicine, in the present paper we revisit this classic mechanical problem and formulate its corresponding inverse. If for a hollow structure (such as a sock or the uterus), eversion means simply 'turning inside out', for a complete spherical shell this is possible only preceded by a cut along a diameter and followed by a rejoining that keeps formerly neighbouring points still neighbouring. For a spherical shell made of an isotropic, incompressible, hyperelastic material, Ericksen [2] had proven that the eversion deformation is compatible with the equilibrium equations. Moreover, when the material of the shell is of Mooney-Rivlin type, the everted shell can be maintained in a spherical shape with zero or non-zero uniform normal pressures p_0 applied to the inner and outer shell surfaces.

Even when we start from an unstressed configuration, in the everted state the shell maintains non-vanishing stresses. As shown by Johnson and Hoger [4], the elasticity tensor produced by a small deformation from the everted configuration will depend on the stresses in the everted configuration. In section 2 we will represent this dependence, extending the calculation from the case of residual stresses considered in [4] to the case of initial stresses, and show the important role played by the non-linearity of the material in the relationship between the elasticity tensor and the applied pressure p_0. We represent this dependence for three values of the applied pressure p_0, as well as three choices of the Mooney-Rivlin material constants.

In section 3 we formulate the inverse problem of the everted spherical shell, in which C_1 and C_2, the material constants of the Mooney-Rivlin material, are computed from measurements in the everted configuration. In particular, we analyse the impact that errors in measurements of the eversion constant A or the pressure p_0 have in determining C_1 and C_2. To the best of our knowledge, this is the first time that such a study has been performed. Our results suggest novel experimental protocols that will allow a robust recovery of the mechanical parameters which ultimately will help differentiate between normal and pathological tissues. The paper ends with a section of conclusions. The present work is an expansion of the work presented by the authors in [6].

2. FORMULATION OF THE DIRECT PROBLEM

As in Johnson and Hoger [4], we consider a spherical shell made of a homogenous, isotropic, incompressible, hyperelastic, Mooney-Rivlin material. We denote by R_1 and R_2 the internal and external shell radius, with $\mathcal{B}_0$ the relaxed, stress free configuration of the shell and with $\mathcal{B}_1$ the shell configuration after an eversion. The eversion deformation maps the material coordinates R, Θ, Φ in the spatial coordinates r, θ, φ as follows:

$$r = (A - R^3)^{1/3}\,,\ \theta = \pi - \Theta\,,\ \phi = \Phi\,, \tag{1}$$

where π is the constant 3.14.., $R_1 \le R \le R_2$, $0 \le \Phi < 2\pi$ and $0 \le \Theta < \pi$, and the constant $A > R_1^3$.

Through deformation (1) the surfaces initially at R_1, R_2 are transformed in the surfaces at r_1, r_2 respectively, with $R_1 < R_2$ and $r_1 > r_2$. In physical (spherical) coordinates, the gradient of deformation (1) $[F_1]$ has the form:

$$[F_1] = \begin{bmatrix} -R^2/r^2 & 0 & 0 \\ 0 & -r/R & 0 \\ 0 & 0 & r/R \end{bmatrix}, \tag{2}$$

and the corresponding left Cauchy-Green deformation tensor $[B_1]$ and its inverse are given by:

$$[B_1] := \left[F_1 F_1^T\right] = \begin{bmatrix} R^4/r^4 & 0 & 0 \\ 0 & r^2/R^2 & 0 \\ 0 & 0 & r^2/R^2 \end{bmatrix},\ \left[B_1^{-1}\right] = \begin{bmatrix} r^4/R^4 & 0 & 0 \\ 0 & R^2/r^2 & 0 \\ 0 & 0 & R^2/r^2 \end{bmatrix}. \tag{3}$$

The strain energy function for a Mooney-Rivlin material is:

$$\hat{\sigma} = C_1(I-3) + C_2(II-3)\,, \tag{4}$$

with C_1, C_2 material constants and I, II the first two invariants of deformation (1):

$$I = tr\ B_1\,, II = 1/2\left[\left(tr\ B_1\right)^2 - tr\ B_1^{\ 2}\right]. \tag{5}$$

The constitutive equation for incompressible, isotropic, hyperelastic materials is:

$$T_1 = -p\,1 + \alpha_1\,B_1 + \alpha_{-1}\,B_1^{-1}\,, \tag{6}$$

where the alpha coefficients depend on the strain energy function as follows:

$$\alpha_1 = 2\frac{\partial\hat{\sigma}}{\partial I}\left(I_1,\, II_1\right),\ \alpha_{-1} = -2\frac{\partial\hat{\sigma}}{\partial II}\left(I_1,\, II_1\right). \tag{7}$$

Computing (7) for the Mooney-Rivlin strain energy (4) and substituting in (6), we obtain the following form for the stress due to eversion:

$$T_1 = -p\,1 + 2\,C_1\,B_1 - 2\,C_2\,B_1^{-1}. \tag{8}$$

As seen in (3), $[B_1]$ and $[B_1^{-1}]$ have diagonal forms in the physical system of coordinates, and from (8) this is also true for T_1. In fact, from (3) and (6) we obtain the following physical components of stress:

$$T_1\langle\theta\theta\rangle = T_1\langle\phi\phi\rangle,\ T_1\langle r\theta\rangle = T_1\langle r\phi\rangle = T_1\langle\theta\phi\rangle = 0. \tag{9}$$

In the everted configuration, $\mathcal{B}_1$, the body is still in equilibrium. Using (9), the equilibrium equations (in physical coordinates) reduce to $p = p(r)$ and

$$\frac{\mathrm{d}T_1\langle rr\rangle}{\mathrm{d}r} = \frac{2}{r}\left(T_1\langle\theta\theta\rangle - T_1\langle rr\rangle\right). \tag{10}$$

Substituting (6) and (7) in equation (10), as well as a reversed chain rule for the strain energy, we obtain the integral form:

$$T_1\langle rr\rangle\big|_r = \int_{r_1}^{r}\frac{\left(A-\rho^3\right)}{A}\frac{\partial\hat{\sigma}}{\partial\rho}\,d\rho + T_1\langle rr\rangle\big|_{r_1}, \tag{11}$$

where r is the radius at a point in the shell wall and ρ is an integration variable.

Until now we have not used any boundary conditions for the spherical shell. We assume further that the stress on the internal and the external surfaces of the shell are equal to a given pressure p_0 where, unlike Johnson and Hoger [4], p_0 can be non-zero. Substituting this boundary condition in (11) and rewriting this integral over the undeformed domain, we obtain:

$$\int_{R_1}^{R_2}\frac{R^3}{A}\frac{\partial\hat{\sigma}}{\partial R}\,\mathrm{d}R = g(A,\ R_2) - g(A,\ R_1) = 0, \tag{12}$$

where $g(A, R)$ was calculated after a tedious integration as:

$$g(A,R) = C_1\frac{\left(5R^4 - 4AR\right)}{\left(A-R^3\right)^{4/3}} + C_2\frac{\left(2A-R^3\right)}{R\left(A-R^3\right)^{2/3}}. \tag{13}$$

As shown by Ericksen in [1], for given C_1, C_2, R_1, R_2, there exists a unique value of A that satisfies both (12) and $A>R_1^3$. With A known, (11) can be written explicitly as:

$$T_1\langle rr\rangle\big|_r = g(A,R) - g(A,R_1) + p_0, \tag{14}$$

where R is transformed through eversion in r. Finally, comparing (14) and the radial component of (8), we can obtain the following expression for the pressure:

$$p(r) = 2C_1\frac{R^4}{\left(A-R^3\right)^{4/3}} - 2C_2\frac{\left(A-R^3\right)^{4/3}}{R^4} - g(A,R) + g(A,R_1) - p_0. \tag{15}$$

With configuration $\mathcal{B}_1$ perfectly determined, let us turn our attention to an infinitesimal deformation of $\mathcal{B}_1$ into a new configuration $\mathcal{B}_2$. As shown in [4], the state of stress in the new configuration will depend both on the deformation from $\mathcal{B}_1$to $\mathcal{B}_2$.and the state of stress in $\mathcal{B}_1$, through

$$T = -p\,1 + T_1 + \left(W_2 T_1 - T_1 W_2\right) + \zeta_c\left[E_2\right]. \tag{16}$$

Here E_2 and W_2 are the symmetric and anti-symmetric part, respectively, of the displacement gradient H_2:

$$H_2 = F_2 - 1\,,\ E_2 = \frac{1}{2}\left(H_2 + H_2{}^T\right),\ W_2 = \frac{1}{2}\left(H_2 - H_2{}^T\right). \tag{17}$$

It can be shown that the elasticity tensor $\zeta_c\left[E_2\right]$ simplifies for this case to:

$$\zeta_c\left[E_2\right] = \left(\Lambda 1 + \mathrm{M} T_1 + \mathrm{N} T_1{}^2\right) E_2 + E_2\left(\Lambda 1 + \mathrm{M} T_1 + \mathrm{N} T_1{}^2\right), \tag{18}$$

with $\Lambda, \mathrm{M}, \mathrm{N}$ some expressions of C_1, C_2, p, I and II, as given in Johnson and Hoger [4].

Using three numerical examples, we will show further how the elasticity tensor $\zeta_c\left[E_2\right]$ depends on initial stresses. We consider R_1=1 cm, R_2=2 cm and different Mooney- Rivlin material constants C_1, C_2. The computed values for the eversion constant A, the everted radii and the pressure on boundaries (up to the choice of p_0) are presented in Table 1, while the dependence of the elasticity tensor on the initial stress is presented graphically in Fig. 1.

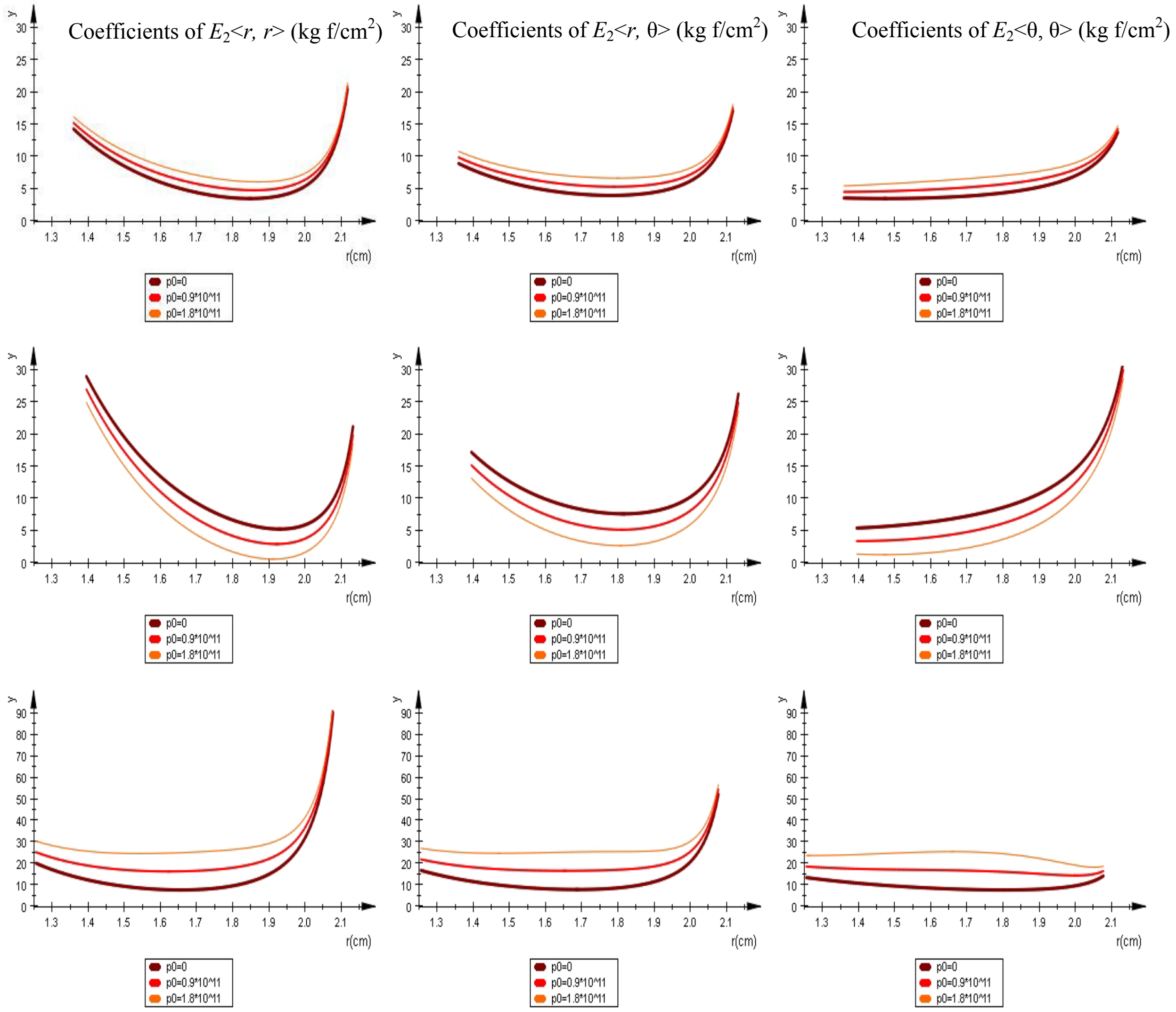

Fig. 1 – Variation of elasticity tensor coefficients with respect to everted radius r for different values of the pressure p_0 = 0 kg f/cm^2, 0.9 · 10^{11} kg f/cm^2, 1.8 · 10^{11} kg f/cm^2. Top row C_1=0.75 kg f/cm^2, C_2=0.25 kg f/cm^2, middle row C_1=1.70 kg f/cm^2, C_2=0.25 kg f/cm^2, bottom row C_1=0.75 kg f/cm^2, C_2=1.2 kg f/cm^2. The case p_0=0 kg f/cm^2 corresponds to the residual stress case of [4].

We notice that the case $p_0 = 0$ kg f/cm^2, corresponding to the presence of residual stresses in the shell, is in agreement with the results presented by Johnson and Hoger [4]. In addition, the elasticity tensor coefficients vary little with p_0 compared with the variation through the radius of the shell. Moreover, compared with Case 1 (see Table 1), the magnitude of the variation, both with respect to the shell radius and to p_0, increases with increasing C_1 (Case 2) or C_2 (Case 3). Even if Cases 2 and 3 conserve a combination of the material constants ($C_1 + C_2 = 1.95$ which represents 1/2 of the shear modulus G of the corresponding linearized elastic constitutive model, see [1]), a variation in C_2 produces a larger variation in magnitude of the elasticity tensor coefficients compared with a similar variation in C_1.

Table 1

Three numerical cases: computed eversion constant A, everted radii r_1 and r_2, and boundary pressures for three given pairs of material constants C_1, C_2

Case #	C_1 (kg f/cm^2)	C_2 (kg f/cm^2)	A (cm)	r_1 (cm)	r_2 (cm)	$p_1=p(r_1)$ (kg f/cm^2)	$p_2=p(r_2)$ (kg f/cm^2)
1	0.75	0.25	10.5189	2.1193	1.3606	-10.0124	6.8957
2	1.70	0.25	10.7222	2.1343	1.3963	-10.2112	14.1934
3	0.75	1.20	9.9848	2.0789	1.2567	-44.7483	9.2477

3. INVERSE PROBLEM FORMULATION

In this section we formulate the inverse problem for the eversion of the spherical shell presented previously. We presume known the value of the pressure $p(r)$ on one of the surfaces of the shell (either $R=R_1$ or $R=R_2$) and the value of the eversion constant A, and we look for the material constants C_1, C_2. For this, we consider the linear system of two equations with the unknowns C_1, C_2 formed by equations (12) and (15) at the chosen radius. While the mathematical problem of finding C_1, C_2 is well determined, only some of its solutions have physical meaning. According to Truesdell and Noll [7] and Beatty [1], based on empirical evidence we must have $C_1 > 0$, $C_2 \geq 0$.

In what follows, we study how a measurement error in A or p influences the accuracy of the computed constants C_1, C_2. Throughout this study we keep constant the initial geometric body, that is the undeformed spherical shell of radii $R_1 = 1$ cm, $R_2 = 2$ cm. We first consider the numerical case $A = 10.5189$ cm and $p_1 = p(R_1) = -10.0123$ kg f/cm^2 and recover $C_1 = 0.75$ kg f/cm^2, $C_2 = 0.25$ kg f/cm^2, the same values that we used in the direct problem, Case 1, above. We repeatedly solve for C_1, C_2 when A and p_1 are within 5% of their nominal values and present in Fig. 2 top, the errors in C_1, C_2 with respect to their nominal values. We observe that C_1 is especially sensitive to errors in A, and a 5% measurement error in A produces almost 950% absolute errors in C_1 and, in fact, a negative value that has no physical sense.

We repeat the study in a few other cases, modifying the point where the pressure is measured (i.e. $p_1 = p(R_1)$ or $p_2 = p(R_2)$), and the values for A and pressure. When $A = 10.5189$ cm and $p_2 = 6.8956$ kg f/cm^2, we recover $C_1 = 0.75$ kg f/cm^2, $C_2 = 0.25$ kg f/cm^2, but as shown in Fig. 2 bottom, the errors in C_1, C_2 are moderate. Once again we observe that an error of 5% in A gives unphysical (negative) values for C_2.

Comparing the top and bottom of Fig. 2 we conclude that, if possible, we prefer to measure p_2 since the resulting errors for C_1 and C_2 would be smaller in this case. We will examine whether this conclusion is true for the other considered values of the eversion constant and of the pressure.

When $A = 10.7222$ cm and $p_1 = -10.2112$ kg f/cm^2, we recover $C_1 = 1.7$ kg f/cm^2, $C_2 = 0.25$ kg f/cm^2 as used in the direct problem, Case 2. We repeatedly solve for C_1, C_2 when A and p_1 are within 5% of their nominal values and present in Fig. 3 top, the errors in C_1, C_2 with respect to their nominal values. As above, we observe that C_1 is especially sensitive to errors in A, and a 5% measurement error in A produces large errors in C_1 and, in fact, a negative value that has no physical sense. We repeat the study for $p_2 = 14.1934$ kg f/cm^2 obtaining the same constants C_1, C_2. Once again we prefer to measure p_2 instead of p_1 since the resulting errors for C_1 and C_2 would be smaller in this case.

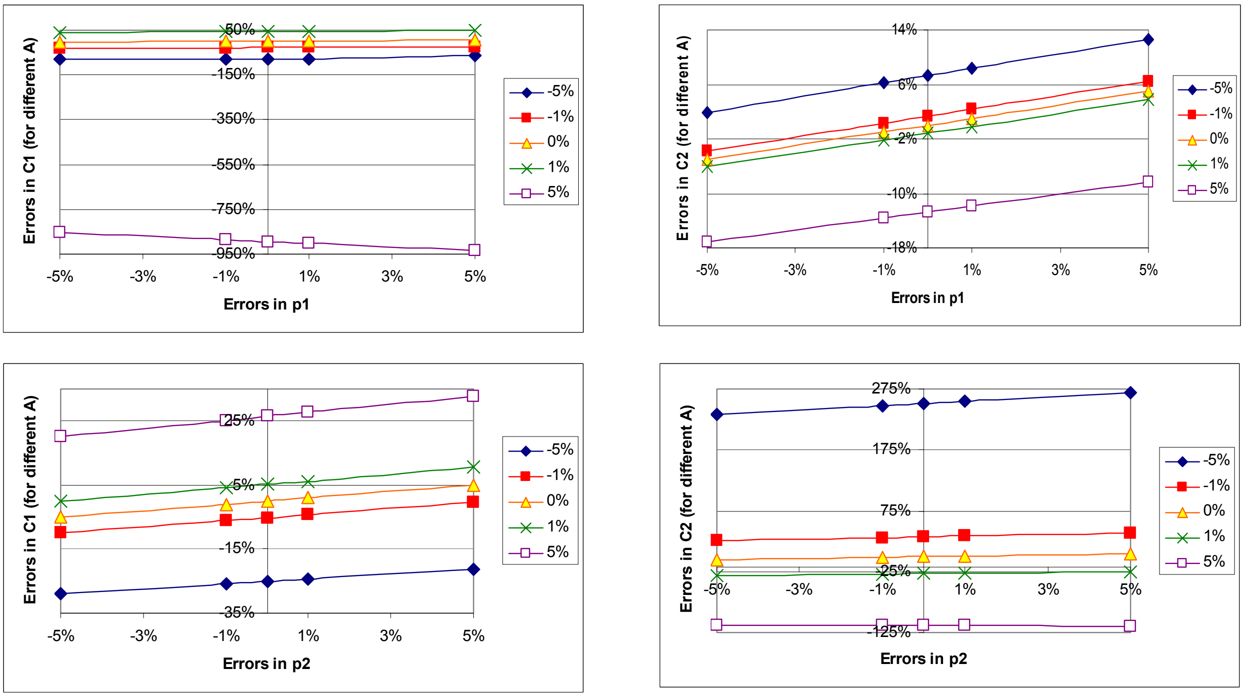

Fig. 2 – Percent errors for constants C_1 and C_2, for up to 5% errors in A= 10.5189 cm and p_1 = –10.0123 kg f/ cm^2 (Case 1.1, top) and p_2 = 6.8956 kg f/ cm^2 (Case 1.2, bottom).

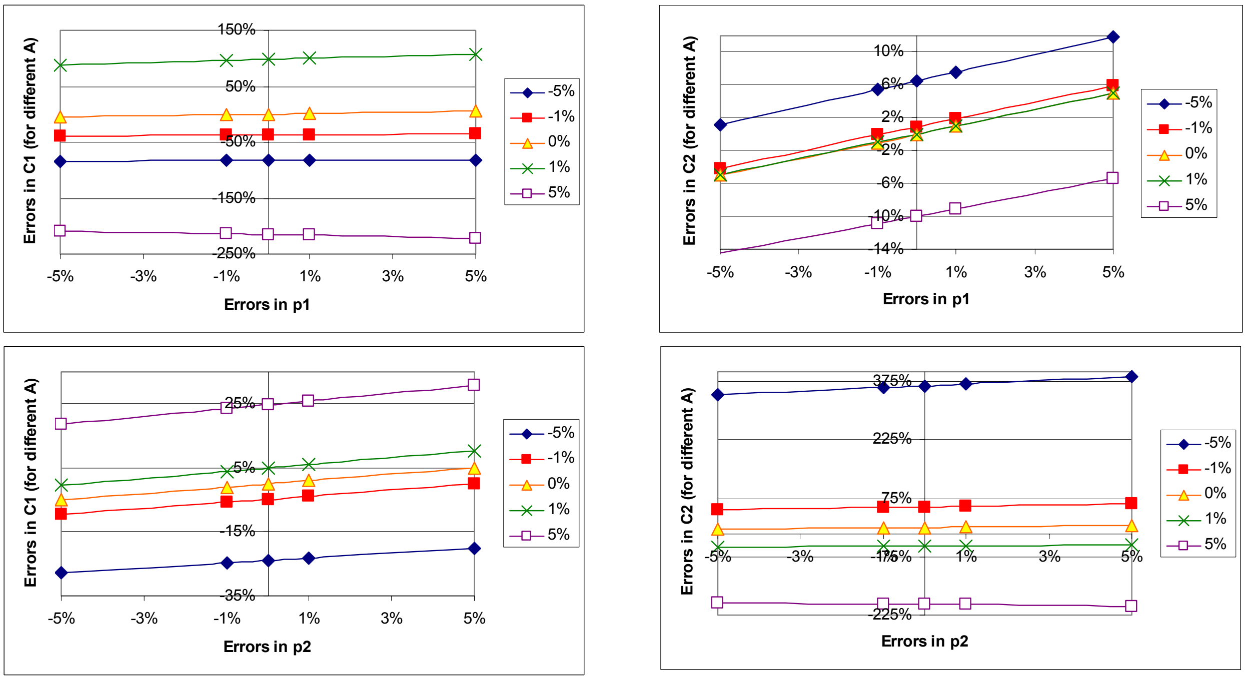

Fig. 3 – Percent errors for constants C_1 and C_2, for up to 5% errors in A = 10.7222 cm and p_1 = –10.2112 kg f/ cm^2 (Case 2.1, top) and p_2 = 14.1934 kg f/ cm^2 (Case 2.2, bottom).

Finally, for A =9.9848 cm and p_1= –44.7483 kg f/cm^2, we recover C_1=1.7 kg f/cm^2, C_2=0.25 kg f/cm^2 as used in the direct problem, Case 3. We repeatedly solve for C_1, C_2 when A and p_1 are within 5% of their nominal values and present in Fig. 4 top, the errors in C_1, C_2 with respect to their nominal values. In contrast with the previous cases, now all values computed for C_1, C_2 have physical meaning.

We repeat the analysis for A = 9.9848 cm and p_2 = 9.2477 kg f/ cm^2 and plot the results in Fig. 4, bottom. Once again all computed values have physical meaning, but this time the errors are larger than in Case 3.1. Based on this example, we could not recommend whether to measure the pressure at R_1 or at R_2.

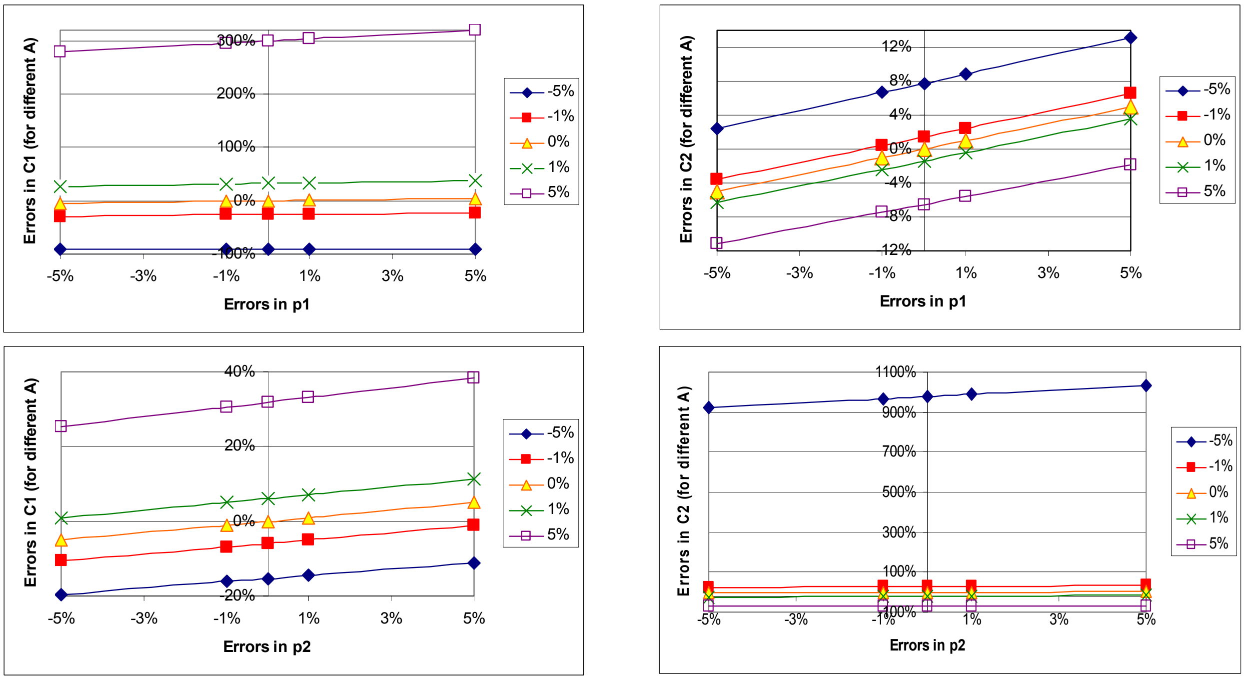

Fig. 4 – Percent errors for constants C_1 and C_2, for up to 5% errors in A =9.9848 cm and p_1 = –44.7483 kg f/ cm^2 (Case 3.1, top) and p_2 = 9.2477 kg f/ cm^2 (Case 3.2, bottom).

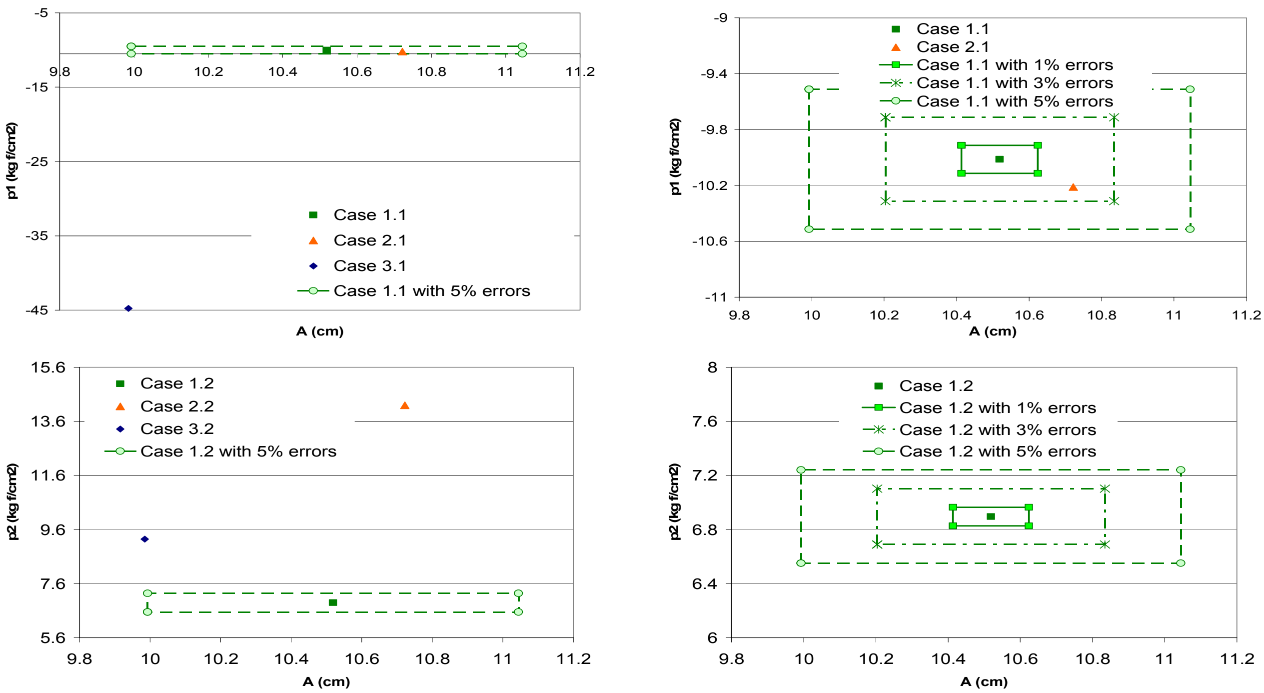

Fig. 5 – Representation of the three cases in the eversion constant-pressure space. When the couple $A - p_1$ is measured as input for the inverse problem, cases 1-2 cannot be distinguished with measurement errors of 2% or more; the same relative error have no confounding effect on the three cases represented in the space $A - p_2$. Figures on right are zoom-in of figures on the left.

To elucidate the question, we plot the three cases in the space eversion constant-pressure ($A - p$). As it can be seen in Table 1, the values of the pressure p_1 for the Cases 1 and 2 of the direct problem are very close, even if C_1 most than doubled. In order to see how close those cases are, we represent in Fig. 5, top left, the Cases 1.1–3.1 as points, as well as the rectangular box containing all measurements with 5% relative errors from the Case 1.1. In Fig. 5 top right, we zoom around the Case 1.1 and represent also the rectangles of Case 1.1 with 1%, 3% and 5% measurement errors. We use a similar representation for the corresponding cases in the $A - p_2$ space in Fig. 5, bottom.

We observe that when the couple $A - p_1$ is measured as input for the inverse problem, having measurement errors of 2% or more do not let us distinguish between Cases 1 and 2 (Fig. 5 top), while case 3 is clearly identified (Fig. 5 top left). In contrast, the same percentage error has no confounding effect on the three cases represented in the space $A - p_2$. Based on this observation and the general error behavior in Cases 2 and 3, we recommend measuring the pressure at the internal radius in the everted configuration (R_2).

4. CONCLUSIONS

In this paper we have revisited the eversion problem for a spherical shell and studied, for the first time, the corresponding inverse problem. The spherical shell is made of a homogenous, incompressible, hyperelastic Mooney-Rivlin material. For the direct problem, we expanded the study from [4] to the case of initial stresses, and noticed that the elastic tensor coefficients vary little with variation of the initial stress compared with the variation through the radius of the shell. In the three numerical cases considered, the magnitude of the variation, increases with increasing constant materials C_1 or C_2 and when a combination of the material constants equivalent to constant shear modulus is kept constant, a variation in C_2 produces a larger variation in magnitude of the elasticity tensor coefficients compared with a similar variation in C_1.

For the inverse problem, we studied how a measurement error in the eversion constant or in pressure influences the accuracy of the computed material constants. We found that, in order to minimize the errors in the calculated constants, it is preferable to measure the pressure at the internal radius in the everted configuration ($p_2=p(R_2)$). Our results suggest novel experimental protocols that will allow a robust recovery of the mechanical parameters which ultimately will help differentiate between normal and pathological tissues. We believe that our study, combined with the digital eversion method for medical images can help improve screening, diagnosis, surgical planning and medical education.

REFERENCES

1. BEATTY, M.F., *A Lecture on Some Topics in Nonlinear Elasticity and Elastic Stability*, IMA Preprint Series # 99, Institute for Mathematics and Its Application, Minneapolis, 1984, p. 32.
2. ERICKSEN, J.L., *Inversion of a perfectly elastic shell*, Z. Angew. Math. Mech, **35**, *9–10*, pp. 382–385, 1955.
3. HONG, W., GU, X., QIU, F., JIN, M., KAUFMAN, A., *Conformal virtual colon flattening*, Proc. 2006 ACM Symposium on Solid and Physical Modeling, 2006 pp. 85–93.
4. JOHNSON, B.E., HOGER, A., *The dependence of the elasticity tensor on residual stress*, Journal of Elasticity, **33**, *1–2*, pp. 145–165, 1993.
5. PAIK, D., BEAULIEU, C., KARADI, C., NAPEL, S., *Visualization modes for CT colonography using cylindrical and planar map projections*, J.Comput. Assist. Tomogr., **24**, *2*, pp.179–188, 2000.
6. ROSCA, R., DRAPACA, C., *Direct and Inverse Problems for the Eversion of a Spherical Shell,* Proc. SISOM 2009 (under press).
7. TRUESDELL, C., NOLL, W., *The Nonlinear Field Theories of Mechanics*, Flugge's Handbuch der Physik III/3, Berlin, Heidelberg, New York, Springer-Verlag, pp. 51–53, 1965.
8. ZHAO, J., CAO, L., ZHUANG, T., WANG, G., *Digital eversion of a hollow structure: an application in virtual colonography*, Int. J. Biomed. Imaging, Article ID 763028, 2008.

Received September 2, 2009